Facile Synthesis and Catalytic Properties of Nickel-Based Mixed-Metal Oxides with Mesopore Networks from a Novel Hybrid Composite Precursor†

Xu Xiang, Halidou I. Hima, Hui Wang, and Feng Li*

State Key Laboratory of Chemical Resource Engineering, Beijing University of Chemical Technology, P.O. Box 98, Beijing 100029, P. R. China

Received July 28, 2007. Revised Manuscript Received October 23, 2007

Facile synthesis of high-surface-area nickel-based mixed-metal oxides with interconnected mesopore networks through a novel layered double hydroxide/carbon (LDH/C) hybrid composite precursor route is successfully established. The starting LDH/C composite with interwoven framework structure is assembled by the crystallization of Ni/Al layered double hydroxide simultaneously accompanied by the carbonization of glucose under mild hydrothermal conditions, and subsequently, the formed composite is thermally decomposed to generate mesoporous nickel-based mixed-metal oxides after removal of the carbon. The materials have been characterized by X-ray diffraction (XRD), Fourier transform infrared technique (FT-IR), thermogravimetric and differential thermal analysis (TG-DTA), scanning electron microscopy (SEM), transmission electron microscopy (TEM), and nitrogen sorption measurements. The results elucidate that the specific surface area of calcined LDH/C composite at 450 °C can be as high as 288 $m^2\ g^{-1}$, and decreases gradually with the calcination temperature. The effect of in situ generated carbon as template in the composite precursor is an essential factor to direct the formation of the high-surface-area mixed oxides with interconnected mesopore network. And the porosity of the obtained solids can be dominated by adjusting the calcination temperature of precursors. Furthermore, through catalytic investigations, these as-prepared high-surface-area Ni-based mixed oxides display excellent catalytic activities for the growth of carbon nanotubes in chemical vapor deposition reactions.

Introduction

Inorganic materials with high specific surface areas are of great interest and have found important applications in prevailing fields such as heterogeneous catalysts, functional ceramics, adsorbents, and sensors.[1] For example, high-surface-area metal oxide materials can be expected to have interesting optical, magnetic, or catalytic properties.[2] Generally, such materials are produced by templating technique,[3] sol–gel processing,[4] or microemulsion method.[5] Among them, templating is a versatile pathway that has attracted considerable attention in recent years, because it provides an unprecedented ability to tailor the structural and textural properties, such as pore size distribution and overall porosity, along with the external shape of samples and the size of particles.[6] Up to now, many different templates have been investigated comprehensively to control the growth of materials with the desired characteristics (e.g., porous structure and unique morphology).[7] Because the pioneer work on carbon templating of zeolite materials by Jacobsen et al.,[8] the uses of carbon like activated carbon or carbon aerogels as templates for the synthesis of diverse high-surface-area metal oxides have been achieved.[1b,9] Additionally, Valdés-Solís and co-workers have prepared high-surface-area perovskite- and spinel-type complex oxides using a porous silica xerogel as template.[10] However, a large number of technological and basically scientific issues still remain to be resolved despite the huge research devotion, in view of the unique chemical or physical properties of materials correlated to the structural aspects.

† Part of the "Templated Materials Special Issue".

* Corresponding author. Tel.: 8610-64451226. Fax: 8610-64425385. E-mail: lifeng_70@163.com.

(1) (a) Schüth, F. *Chem. Mater.* **2001**, *13*, 3184. (b) Schwickardi, M.; Johann, T.; Schmidt, W.; Schüth, F. *Chem. Mater.* **2002**, *14*, 3913. (c) Kemnitz, E.; Groβ, U.; Rüdiger, S.; Shekar, C. S. *Angew. Chem., Int. Ed.* **2003**, *42*, 4251.

(2) (a) Sanchez, C.; Lebeau, B.; Chaput, F.; Boilot, J. P. *Adv. Mater.* **2003**, *15*, 1969. (b) Stein, A. *Adv. Mater.* **2003**, *15*, 763. (c) Tosheva, L.; Valtchev, V. P. *Chem. Mater.* **2005**, *17*, 2494. (d) Kondo, J. N.; Uchida, M.; Nakajima, K.; Daling, L.; Hara, M.; Domen, K. *Chem. Mater.* **2004**, *16*, 4304.

(3) Schüth, F. *Angew. Chem., Int. Ed.* **2003**, *42*, 3604.

(4) Zayat, M.; Levy, D. *Chem. Mater.* **2000**, *12*, 2763.

(5) (a) Bumajdad, A.; Zaki, M. I.; Eastoe, J.; Pasupulety, L. *Langmuir* **2004**, *20*, 11223. (b) Teng, F.; Xu, J.; Tian, Z.; Wang, J.; Xu, Y.; Xu, Z.; Xiong, G.; Lin, L. *Chem. Commun.* **2004**, *1858*.

(6) (a) Caruso, R. A. *Top. Curr. Chem.* **2003**, *226*, 91. (b) Polarz, S.; Orlov, A. V.; Schüth, F.; Lu, A.-H. *Chem.—Eur. J.* **2007**, *13*, 592. (c) Rumplecker, A.; Kleitz, F.; Salabas, E.-L.; Schüth, F. *Chem. Mater.* **2007**, *19*, 485.

(7) (a) Yang, P.; Zhao, D.; Margolese, D. I.; Chmelka, B. F.; Stucky, G. D. *Chem. Mater.* **1999**, *11*, 2813. (b) Shchukin, D. G.; Caruso, R. A. *Chem. Mater.* **2004**, *16*, 2287. (c) Yang, C.-M.; Weidenthaler, C.; Spliethoff, B.; Mayanna, M.; Schüth, F. *Chem. Mater.* **2005**, *17*, 355. (d) Sadakane, M.; Asanuma, T.; Kubo, J.; Ueda, W. *Chem. Mater.* **2005**, *17*, 3546.

(8) Jacobsen, C. J. H.; Madsen, C.; Houzvicka, J.; Schmidt, I.; Carlsson, A. *J. Am. Chem. Soc.* **2000**, *122*, 7116.

(9) (a) Li, W.; Lu, A.-H.; Schmidt, W.; Schüth, F. *Chem.—Eur. J.* **2005**, *11*, 1658. (b) Li, W.; Lu, A.-H.; Weidenthaler, C.; Schüth, F. *Chem. Mater.* **2004**, *16*, 5676.

(10) Valdés-Solís, T.; Marbán, G.; Fuertes, A. B. *Chem. Mater.* **2005**, *17*, 1919.

10.1021/cm702072t CCC: $40.75
Published on Web 12/05/2007

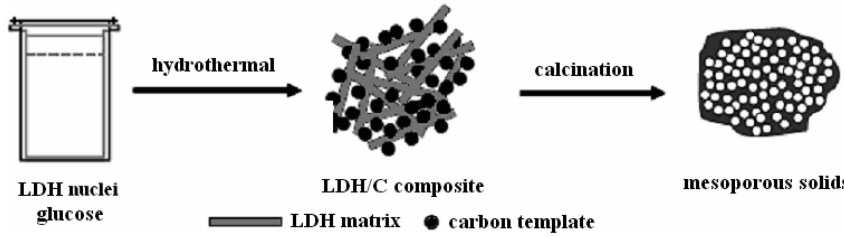

Figure 1. Schematic illustration of the synthesis of high specific surface area Ni-based mixed oxides with interconnected mesopore networks through an in situ generated carbon templating pathway with NiAl-LDH as precursor of resultant mixed oxides and glucose as source of carbon template. In the hydrothermal reactions, the newly formed NiAl-LDH nanocrystallites are hybridized with the in situ generated carbon via carbonization of glucose to form LDH/C composite. After removal of the carbon template by calcination at 450 °C or above in air, Ni-based mixed-metal oxides with high specific surface area and mesopore networks (see Figure 7) are obtained.

Layered double hydroxides (LDHs), $[M^{II}_{1-x}M^{III}_{x}(OH)_2]^{x+}(A^{n-})_{x/n}\cdot mH_2O$, with a brucite ($Mg(OH)_2$)-like layered structure, are a family of synthetic anionic clays that consist of positively charged layers containing alternatively distributed divalent and trivalent cations in the sheets and charge-balancing anions between the layers.[11] Because of the characteristic of tunable compositions and exchangeable anions, the materials of this class have been used as catalysts, catalyst–supports, chemical additives, or stabilizers in polymer composites, drug delivery systems, adsorbents for wastewater treatment, electrode materials, and molecular precursors for chemically tailored functional materials such as spinel ferrites.[12] Especially, calcination of LDHs at intermediate temperatures (450–600 °C) often gives poorly crystallized mixed-metal oxides, which have remarkable properties as catalysts and catalyst supports.[13]

Considerable attention has been paid to LDHs composites or hybrids, most of which were involved with the intercalation attributable to the unique anion exchanging reactivity in the interlayer space of LDHs in the past few years.[14] Recently, a kind of negative carbon replica was obtained through pyrolysis of organo-modified LDHs followed by dissolution of inorganic moiety, where LDH itself as an inorganic framework affected the textural properties of the resultant carbon.[15] Similar studies have been reported on the preparation of montmorillonite−carbon composites by intercalation of sugar within the smectite clay and thus the derived carbon via acid demineralization.[16] Also, a report has described a novel caramel−sepiolite nanocomposite from the starting sucrose−sepiolite mixture and its controlled thermal conversion to a class of carbon−sepiolite nanocomposite.[17] More recently, an in situ carbon-templating approach by sucrose decomposition has been applied for the synthesis of mesoporous zoelites.[18] Therefore, some appropriate carbon-containing molecules like sucrose or glucose can be advantageous precursors for the formation of carbon under mild conditions.

In this report, we successfully developed a new and facile pathway for the preparation of high-specific-surface-area nickel-based mixed oxides with mesopore networks that was obtained by thermal conversion of a Ni/Al layered double hydroxide/carbon (LDH/C) hybrid composite precursor. The preparation is schematically illustrated in Figure 1. In this synthetic strategy, LDH/C composite was assembled by the crystallization of LDH simultaneously accompanied by carbonization of glucose under mild hydrothermal conditions without use of organic toxic reagents. The templating effect of in situ generated carbon, highly dispersed into LDH matrixes, played an important role on the structure and texture of LDH precursor as well as the resultant mixed oxides. This applied carbon-templating approach, which does not need either the participation of complicated intercalation procedure of carbohydrate into anionic layered precursors or the specialized mesoporous templates, greatly enlarges the practical application areas of layered double hydroxides and their derivatives. To the best of our knowledge, there is no report on the LDH/carbon composite materials as precursor for the preparation of mesoporous mixed oxides. Furthermore, because of their high surface areas, the as-prepared nickel-based mixed oxides can give rise to highly dispersed metallic Ni nanoparticles after reduction and thus exhibit excellent catalytic activities for the growth of carbon nanotubes (CNTs) in chemical vapor deposition.

Experimental Section

Synthesis of NiAl-CO_3^{2-}-LDH. The reagents were used as received without further purification. A mixture of $Ni(NO_3)_2\cdot 6H_2O$ and $Al(NO_3)_3\cdot 9H_2O$ was dissolved in 30 mL of deionized water to form a clear solution ($[Ni^{2+}] = 0.2$ M, $[Al^{3+}] = 0.1$ M). The salt solution was rapidly poured into a 30 mL NaOH and Na_2CO_3 solution ($[OH^-] = 0.48$ M, $[CO_3^{2-}] = 0.2$ M) within several seconds under vigorous stirring. The mixture solution was further

(11) (a) Braterman, P. S.; Xu, Z. P.; Yarberry, F. In *Handbook of Layered Materials*; Auerbach, S. M., Carrado, K. A., Dutta, P. K., Eds.; Marcel Dekker: New York, 2004; Chapter 8, pp 373–474. (b) Williams, G. R.; O'Hare, D. *J. Mater. Chem.* **2006**, *16*, 3065. (c) Evans, D. G.; Slade, R. C. T. *Struct. Bonding* **2006**, *119*, 1.

(12) (a) Khan, A. I.; O'Hare, D. J. *Mater. Chem.* **2002**, *12*, 3191. (b) Leroux, F.; Taviot-Guého, C. *J. Mater. Chem.* **2005**, *15*, 3628. (c) Evans, D. G.; Duan, X. *Chem. Commun.* **2006**, 485. (d) Naghash, A. R.; Xu, Z.; Etsell, T. H. *Chem. Mater.* **2005**, *17*, 815. (e) Li, F.; Liu, J.; Evans, D. G.; Duan, X. *Chem. Mater.* **2004**, *16*, 1597.

(13) (a) Carja, G.; Gelahay, G. *Appl. Catal., B* **2004**, *47*, 59. (b) Chellam, U.; Xu, Z. P.; Zeng, H. C. *Chem. Mater.* **2000**, *12*, 650.

(14) (a) Fudala, A.; Palinko, I.; Kiricsi, I. *Inorg. Chem.* **1999**, *38*, 4653. (b) Leroux, F.; Besse, J.-P. *Chem. Mater.* **2001**, *13*, 3507. (c) Gerardin, C.; Kostadinova, D.; Sanson, N.; Coq, B.; Tichit, D. *Chem. Mater.* **2005**, *17*, 6473. (d) Feng, Y. J.; Williams, G. R.; Leroux, F.; Taviot-Guého, C.; O'Hare, D. *Chem. Mater.* **2006**, *18*, 4312.

(15) (a) Leroux, F.; Raymundo-Piñero, E.; Nedelec, J.-M.; Béguin, F. J. *Mater. Chem.* **2006**, *16*, 2074. (b) Leroux, F.; Dubois, M. *J. Mater. Chem.* **2006**, *16*, 4510.

(16) Bakandritsos, A.; Steriotis, Th.; Petridis, D *Chem. Mater.* **2004**, *16*, 1551.

(17) Gómez-Avilés, A.; Darder, M.; Aranda, P.; Ruiz-Hitzky, E. *Angew. Chem., Int. Ed.* **2007**, *46*, 923.

(18) Kustova, M.; Egeblad, K.; Zhu, K.; Chistensen, C. H. *Chem. Mater.* **2007**, *19*, 2915.

stirred for 20 min at room temperature. Subsequently, the suspension was centrifuged, washed, and redispersed in deionized water for 5 cycles to remove residue salts and alkali, a similar procedure to the latest report of LDH synthesis.[19] The resulting precipitate was transferred into a Teflon-lined autoclave (90 mL total volume), and the deionized water of 80 mL was added to it. The autoclave was then tightly sealed and maintained at 150 °C for a period of 10 h. The resulting bluish green suspension was directly dried in an oven at 70 °C to collect the solid powder Ni/Al-LDH product.

Synthesis of LDH/C Composite and Resultant Mixed Oxides. Analytical-grade glucose ($C_6H_{12}O_6$) was dissolved in 30 mL of deionized water to form a clear solution with a molar ratio of $C_6H_{12}O_6$:(Ni^{2+}+Al^{3+}) = 2.5:1. The precipitate obtained via the above-mentioned room-temperature coprecipitation was dispersed in the glucose solution and placed in an ultrasonic cell for 20–30 min. The mixture solution was transferred into an autoclave with the same fill volume and maintained at the same temperature and period (150 °C, 10 h). The resulting brown product was centrifuged and washed with deionized water five times and then washed with ethanol five times. The final LDH/C product was collected after an oven-dried process at 70 °C for more than 8 h. The dried LDH and LDH/C composite powders were loaded to crucible with cover and thus calcined under an air atmosphere in a temperature-controlled furnace (ramp: 10 °C/min) to produce mixed-metal oxides. The pristine LDHs calcined at 450, 600, and 700 °C were labeled L450, L600, and L700, respectively, and LDH/C composites calcined at 450, 600, and 700 °C were labeled C450, C600, and C700, respectively. For further insights on the structural transformation of calcined LDH and LDH/C composite after reduction, the calcined samples at 450 and 600 °C were subject to a reduction treatment under a flow of 10:1 N_2:H_2 at 500 °C for 40 min. The reduced samples were labeled L450RE, L600RE, C450RE, and C600RE.

Growth of CNTs. The growth of CNTs was achieved in a quartz tube reactor inside a tube furnace equipped with mass controller and temperature-programmed apparatus by catalytic chemical vapor deposition of acetylene. A certain amount of calcined powders was loaded into an alumina boat and positioned in the middle of the quartz tube. At first, the tube furnace was heated to 500 °C at a rate of 5 °C/min under a N_2 gas flow of 60 mL/min. The temperature was maintained at 500 °C for 40 min under a constant flow of N_2/H_2 gas mixture with a ratio of 10:1. The H_2 gas was then switched off and the temperature was further raised to 700 °C. The furnace was held at 700 °C for 90 min under a flow of N_2/C_2H_2 gas mixture with a ratio of 10:1. After the reaction was finished, the flow of N_2 gas was continued and the furnace was cooled to room temperature. Finally, a black powder product was collected from the alumina boat. Further, the product was purified in an aqueous solution of hydrogen chloride for 7 days followed by washing with a large amount of deionized water until the pH value is 7.

Characterization. Powder X-ray diffraction (XRD) patterns of the samples were collected using a Shimadzu XRD-6000 diffractometer under the following conditions: 40 kV, 30 mA, graphite-filtered Cu*K*α radiation (λ = 0.15418 nm). The samples, as unoriented powders, were step-scanned in steps of 0.04° (2θ) using a count time of 10 s/step. The observed diffraction peaks were corrected using elemental Si as an internal standard (d(111) = 0.31355 nm; JCPDS card 27–1402).

Thermogravimetric and differential thermal analysis (TG-DTA) were achieved on a Perkin-Elmer Diamond thermal analysis system with an elevating rate of 10 °C /min from room temperature to 800 °C in air atmosphere.

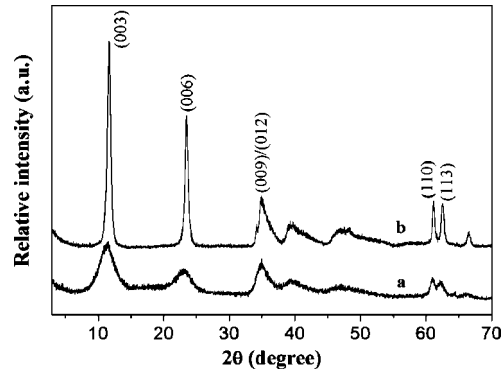

Figure 2. XRD patterns of (a) LDH/C composite and (b) LDH.

Elemental analysis (C and H content) was performed using an elemental analyzer (Elementarvario EL) with sensitivity of 0.3%.

Room-temperature Fourier transform infrared (FT-IR) spectra were obtained on a Bruker Vector-22 Fourier transform spectrometer over the wavelength range 4000 to 400 cm^{-1} with a 2 cm^{-1} resolution, and the sample was prepared by using the KBr pellet method.

The specific surface area determination and pore size and volume analysis were performed by BET and BJH methods from the N_2 adsorption measurements at 77 K using a static volumetric Quantachrome Autosorb-1C-VP Analyzer. Prior to the measurements, samples were degassed at 200 °C for a period of 2 h.

The morphology and structure of samples were characterized by a Hitachi S4700 field-emission scanning electron microscopy (FESEM). The powder sample was stuck to carbon glue on a sample holder and sputtered with a conductive layer of Pt to enhance the conductivity before observations.

The microstructure of samples was investigated on a Hitachi H-800 transmission electron microscopy (TEM) at an accelerating voltage of 150 kV. For TEM observations, the synthesized sample was ultrasonically dispersed in an appropriate amount of ethanol and a drop of the resulting suspension was deposited on a carbon-coated Cu grid followed by the evaporation of solvent in air.

The Raman spectra were collected at room temperature using a Raman spectrometer (Jobin Yvon Horiba HR800). The 532 nm laser was used as excitation source.

Results and Discussion

Characterization of LDH/C Composite. NiAl−LDH with interlayer carbonate anions and NiAl−LDH/C composite were prepared using the conventional coprecipitation technique assisted by a mild hydrothermal process. A Ni/Al ratio of 2.0 was employed in the synthesis mixture. Figure 2 presents XRD pattern of the samples. The pristine LDH sample displays the characteristic diffraction peaks corresponding to hydrotalcite-like LDH family, i.e.. (003), (006), (012), (110). and (113),[20] whereas the intensive and sharp diffraction peaks reveal the highly crystalline nature and excellent layered feature of the sample. In contrast, the broadened diffractions of the LDH/C composite appear almost at the same 2θ positions as those of pure LDH. No crystalline carbon-related diffractions are detected, suggesting that most of carbon products exist in the form of amorphous phase. Here, the carbon product acts as diluent of crystalline

(19) Xu, Z. P.; Stevenson, G. S.; Lu, C.-Q.; Lu, G. Q.; Bartlett, P. F.; Gray, P. P. *J. Am. Chem. Soc.* **2006**, *128*, 36.

(20) Zhao, Y.; Li, F.; Zhang, R.; Evans, D. G.; Duan, X. *Chem. Mater.* **2002**, *14*, 4286.

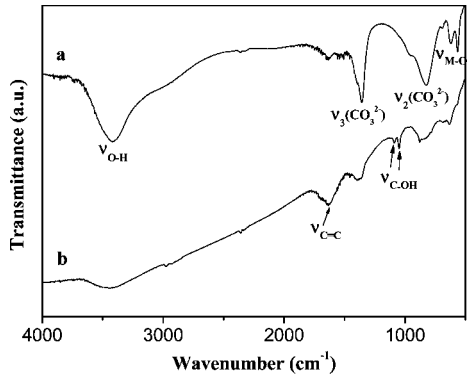

Figure 3. FT-IR spectra of (a) LDH and (b) LDH/C composite.

LDH phase, and hence the intensity of diffraction lines of the LDH/C composite decreases to some extent. The present reaction temperature of 150 °C is higher than the normal glycosidation temperature of glucose, thus leading to aromatization and carbonization of glucose under the hydrothermal conditions.[21] After the chemical reactions of glucose, the resultant organic compounds such as oligosaccharides can be removed by washing many times with large amounts of water and alcohol. Therefore, the resulting hydrothermal is defined as layered double hydroxide/carbon composite. The lateral crystallite sizes of LDH in the forms of pure compound and hybrid composite are estimated to be 21.4 and 10.6 nm, respectively, according to Scherrer's formula.[20] A distinct shrinkage of the crystallite size in LDH/C composite may be attributable to the confined effect of carbon on the LDH crystallite size during the crystallization. Considering that crystal growth requires advancing of grain boundaries,[22] the crystal growth can be effectively inhibited by introducing secondary-phase particles along grain boundaries, which has been validated in the sol–gel synthesis of nanocrystalline metal oxides.[23] In our case, because of the fact that carbon is concurrently in situ generated along with the crystallization of LDH particles, carbon particles as a "co-generated template" can be hybridized with LDHs sheets at grain boundaries and thereby restrain the growth of LDH crystallites.

The formation of LDH/C composite is also supported by the FT-IR results. The FT-IR spectra of pure LDH and LDH/C composite in the region between 4000 and 500 cm^{-1} are illustrated in Figure 3. For pristine LDH, a broad absorption band around 3600–3200 cm^{-1} centered at 3420 cm^{-1} corresponds to the O−H stretching vibrations of hydroxyl groups of brucitic layers and interlayer water molecules. Two intense absorption bands peaked at 1357 and 825 cm^{-1} are attributable to the symmetric stretching vibrations (ν_3) and out-of-plane deformation (ν_2) of carbonate

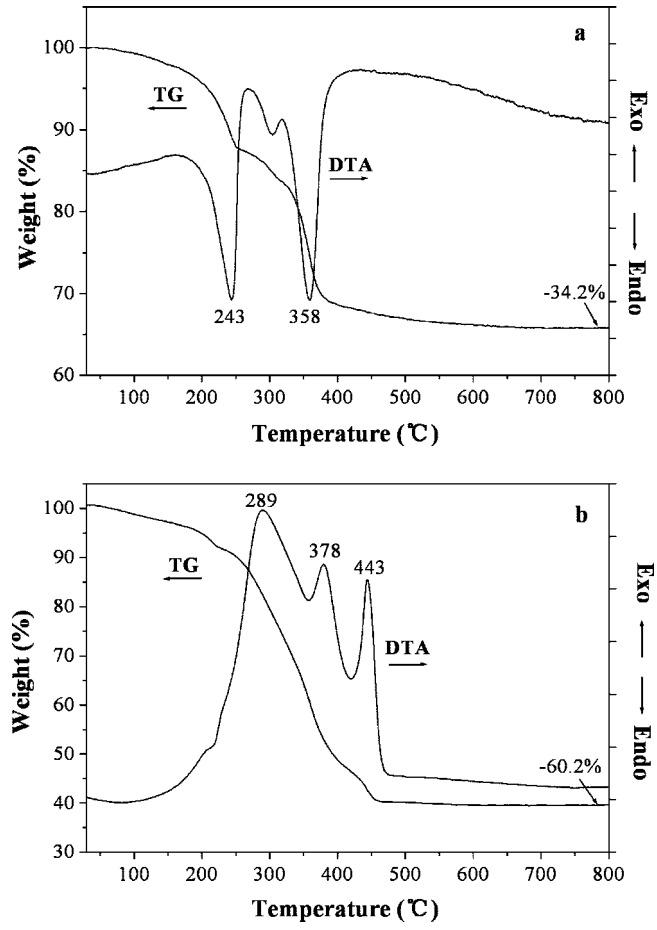

Figure 4. TG-DTA curves of (a) LDH and (b) LDH/C composite.

ions,[24] indicative of the characteristic of interlayer carbonate anions. The other bands observed in the lower frequency region of the spectrum, around 650–530 cm^{-1}, are attributed to metal–oxygen and metal−hydroxyl vibrations in the lattice of LDHs. In contrast, the spectrum of LDH/C composite sample presents a new vibration mode at 1627 cm^{-1}, which can be assigned to the *C*═C asymmetric stretching vibration.[21a] Additional bands in the range of 1000–1100 cm^{-1} involve the C−OH stretching and O−H bending vibrations, implying the existence of residue hydroxyl groups. Although the bands corresponding to O−H and carbonate ion vibrations of LDH itself are retained, the intensities have been greatly decreased because of the hybrid characteristic of the LDH/C composite.

The thermal behavior of samples is studied by TG-DTA analysis. As commonly for LDHs, the weight loss for the Ni/Al−LDH sample takes place apparently in two stages below 400 °C (Figure 4a).[11] The first one with a weight loss of about 12%, accompanied by an intensive endothermic peak at 243 °C in the DTA curve, can be assigned to removal of water physisorbed on the external surface of the crystallites as well as water intercalated in the interlayer galleries. The second weight loss of approximately 18% occurs above 280 °C and involves dehydroxylation of the layers as well as the loss of volatile species CO_2 arising from the interlayer CO_3^{2-} ions. The corresponding DTA curve shows a sharp

(21) (a) Sun, X.; Li, Y. *Angew. Chem., Int. Ed.* **2004**, *43*, 597. (b) Sakaki, T.; Shibata, M.; Miki, T.; Hirosue, H.; Hayashi, N *Bioresour. Technol.* **1996**, *58*, 197. (c) Luijkx, G. C. A.; van Rantwijk, F.; van Bekkum, H.; Antal Jr, M. J *Carbonhydr. Res.* **1995**, *272*, 191. (d) Wang, Q.; Li, H.; Chen, L.; Huang, X. *Carbon* **2001**, *39*, 2211. (e) Wang, Q.; Li, H.; Chen, L. Q.; Huang, X. J. *Solid State Ionics* **2002**, 152–153, *43*.

(22) Chiang, Y. Y. M.; Birnie, III, D. P.; Kingery, W. D. *Physical Ceramic−Principles for Ceramic Science and Engineering*; John Wiley and Sons: New York, 1997.

(23) Wu, N.-L.; Wang, S.-Y.; Rusakova, I. A. *Science* **1999**, *285*, 1375.

(24) Ogawa, M.; Kaido, H. *Langmuir* **2002**, *18*, 4240.

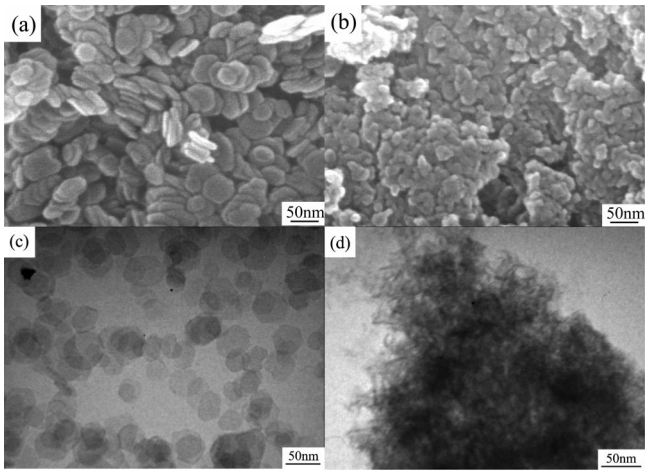

Figure 5. SEM images of (a) LDH and (b) LDH/C composite, and TEM photographs of (c) LDH and (d) LDH/C composite.

endothermic maximum at 358 °C. The further weight loss events that occur at slightly higher temperature are usually ascribed to the removal of strongly held hydroxyl groups onto brucite-like layers. In comparison, the LDH/C composite shows a distinctly different thermal behavior (Figure 4b). The major weight loss events also occur in two stages. The first one below 220 °C, accompanied by a rather small endothermic peak at 213 °C in the curve of DTA, corresponds to the stepwise elimination of physisorbed and intercalated water molecules in LDH crystallites. The weakened endothermic feature can be due to the initial oxidation occurrence of carbon in air atmosphere, apparently causing a reverse thermal effect. In the second weight-loss stage between ca. 220 and 450 °C, the intensive exothermic effect observed in DTA curve shows three peaks at around 289, 378. and 443 °C, respectively, indicative of stepwise oxidation of carbon with elevated temperature. The involved temperature range overlaps that of LDH, where the distinct endothermic events commonly take place, and the oxidation of carbon shows a much more intensive exothermic behavior. Therefore, the endothermic effect of LDH itself is masked to a large extent. In addition, elemental analysis results show the content of carbon and hydrogen in LDH (C, 2.353; H, 3.429 in wt %) and in LDH/C composite (C, 26.86; H, 4.57 in wt %), indicative of the carbon-rich characteristic of the hybrid composite.

Figure 5a displays the morphology of the LDH sample. One can clearly see that the product consists of platelet-like particles with an average size of 40−50 nm and a thin thickness of around 10 nm. The plate-shaped morphology is commonly observed in LDH products with well-crystalline structure. No other morphology is observed in the sample, suggestive of the uniformity of product. In comparison, the morphology of the LDH/C composite is different from the LDH sample (Figure 5b). Only aggregates appear in the image instead of the plate-shaped particles, which can be attributed to the formation of hybrid structure during the growth and crystallization. The TEM observations further reveal the difference between the two samples. It is apparently observed from Figure 5c that most LDH crystallites have hexagonal platelet appearance with an average size of 40−50 nm. These LDH crystallites display light contrast

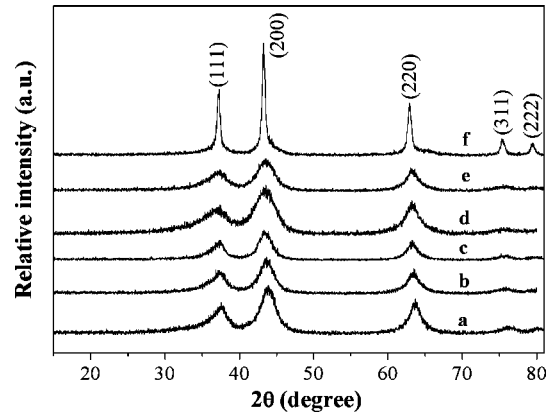

Figure 6. XRD patterns of samples (a) L450, (b) L600, (c) L700, (d) C450, (e) C600, and (f) C700.

because of their thin thickness of about 10 nm. In comparison, only some aggregates with a submicrometer size are observed in LDH/C composite, shown in Figure 5d. Isolated LDH particles are barely found nor the spherical carbon particles, which differs from the products synthesized by just using glucose as reacting agent under similar hydrothermal conditions.[21a] The results indicate that the interaction between LDH crystallites and carbon during the growth leads to a cross-linked hybrid structure consisting of the interwoven LDH particles and noncrystalline carbon.

Characterization of Mixed-Metal Oxides. After heating in air at 450 °C, carbon in LDH/C composite are almost depleted because of the oxidation in view of the above TG-DTA analysis, and simultaneously the layered structure of LDH collapses and converts into mixed-oxide phases. Figure 6 shows XRD patterns of calcined LDH and LDH/C samples at 450, 600, and 700 °C, respectively. One can see that all calcined products exhibit the diffractions of NiO-like Bunsenite phase, which can be easily indexed to cubic NiO phase (JCPDS 47–1049). No other crystalline phases appear in these patterns. However, the broad diffraction peaks presented in Figure 6 a−e reveal the existence of some amorphous products, e.g., alumina or $NiAl_2O_4$ spinel.[25] Furthermore, it is worth noting that the thermal conversion of LDH/C composite at 700 °C leads to the formation of well-crystalline NiO phase (Figure 6f). This may be due to the fact that the hybrid characteristic of carbon with LDH matrix has an effect on the thermal behavior of the LDH material, as evidenced by the above TG-DTA results, and further on the structural transformation from precursor to mixed-metal oxides.

The SEM and TEM images of the mixed oxides derived from LDH/C composite precursor are shown in Figure 7. The SEM image of sample C450 reveals a bulk structure with close interparticulate connections. Upon heating at 600 °C, a similar structure was observed, as displayed in Figure 7b. Sample C600 presents a little more apparent particulate feature than sample C450 because of the removal of carbon products, indicative of the particle size of 30−40 nm. Upon the temperature being further elevated to 700 °C (Figure 7c), the close-connected structure between particles no longer

(25) Rebours, B.; d'Espinose de la Caillerie, J.-B.; Clause, O. *J. Am. Chem. Soc.* **1994**, *116*, 1707.

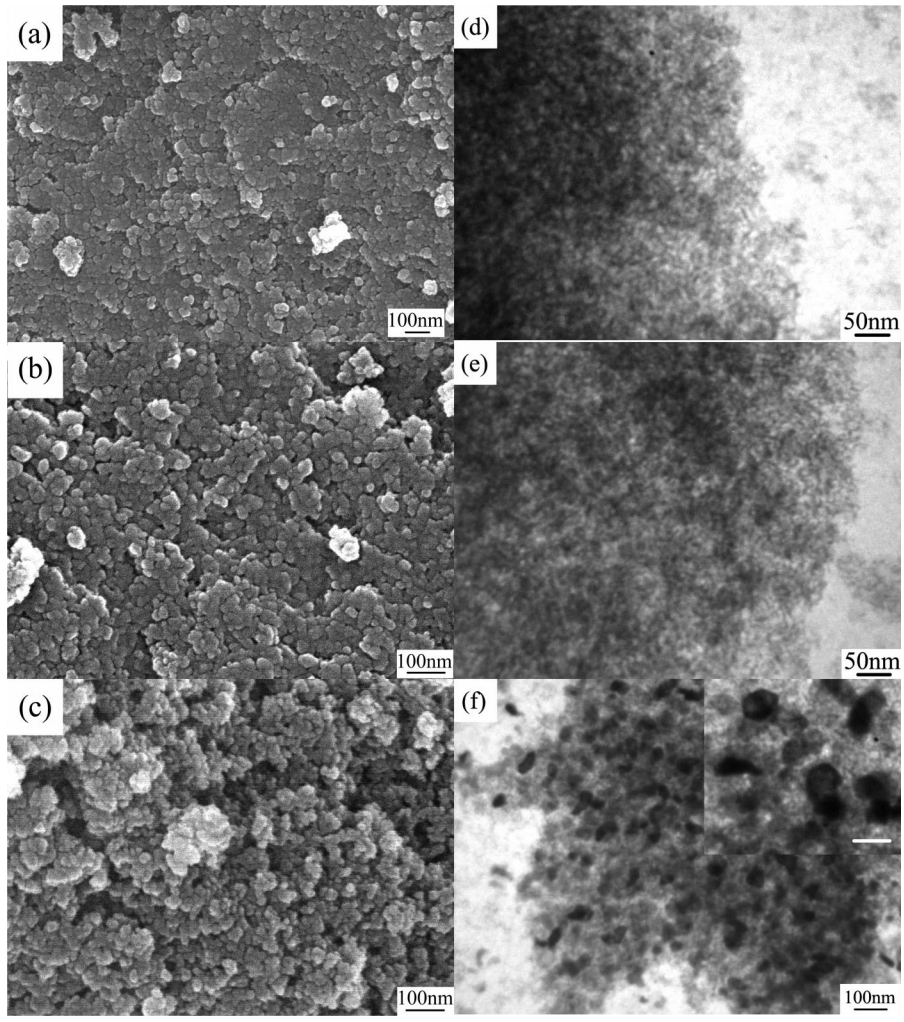

Figure 7. SEM images of samples (a) C450, (b) C600, and (c) C700, and the TEM photographs of sample (d) C450, (e) C600, and (f) C700. The inset of (f) is a magnified view. The scale bar is 50 nm.

exist in the C700, and loose agglomerates of particles appear that are due to recrystallization of NiO phase at high temperature. Correspondingly, TEM observations reveal a more clear structure evolution characteristic for calcined products from LDH/C composite. It can be found that sample C450 exhibits a network structure with interconnected mesopore feature (Figure 7d). This differs from the usual calcined LDHs products, which retained somewhat platelike outline.[13] With a temperature increase to 600 °C, the mesopore network is still maintained, displayed in Figure 7e. However, Figure 7f shows a large number of particles with a size around 40−50 nm formed in the sample C700, indicative of the destruction of the network structure. A magnified view is shown in the inset of Figure 7f, apparently displaying the particles with polyhedral geometry. This is due to the fact that the mesoporous network is destroyed at a higher calcination temperature mostly because of the weakened interactions among particles as well as the better-crystallized structure. The formation of well-defined nanoparticles can partly account for the well-crystalline nature of the product, evidenced by XRD spectra.

Figure 8 shows the nitrogen sorption isotherms of the calcined LDHs and LDH/C composites. The calcined LDHs (Figure 8a) display a type IV isotherm with type H1 hysteresis loops in the relative pressure range of 0.78–0.96.

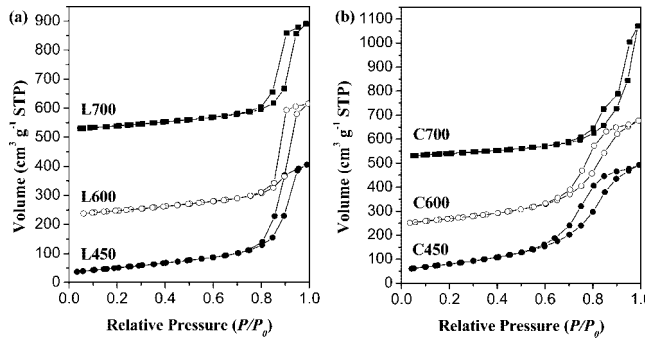

Figure 8. N_2 sorption isotherms of (a) calcined LDH at different temperatures and (b) calcined LDH/C composite at different temperatures. For clarity, the isotherms of L600 and L700 were offset vertically by 200 and 500 cm^3 g^{-1} STP, respectively. The isotherms of C600 and C700 were offset vertically by 200 and 500 cm^3 g^{-1} STP, respectively.

The high relative pressure indicates large pore size in these samples. The pore size distributions were determined by using a Barrett–Joyner–Halenda (BJH) method to the desorption branch of the isotherm. The pore size shows a broad distribution in the range of 2–50 nm for all three samples (Figure 9a). In the case of sample L450, the pores have a primary size distribution above 5 nm, with a maximum at around 17.5 nm. Also, a small portion of pores with a distribution of 2–5 nm has been observed. In contrast, the

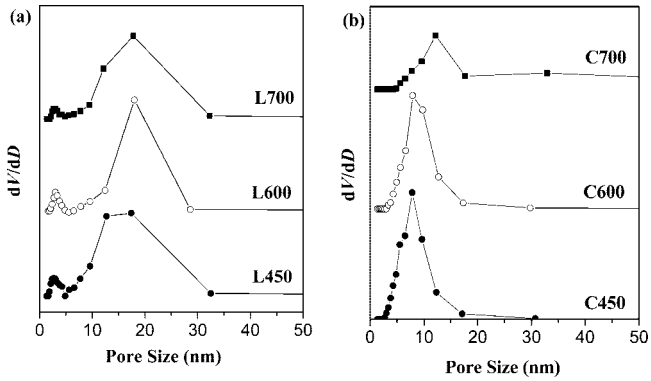

Figure 9. Pore size distributions of (a) calcined LDH at different temperatures and (b) calcined LDH/C composite at different temperatures.

Table 1. Textural Properties of the Mixed Oxides Derived from LDHs and LDH/C Composites[a]

sample	S_{BET} (m^2 g^{-1})	V_p (cm^3 g^{-1})	pore size (nm)
L450	182	0.63	2.8, 17.5
L600	168	0.64	3.0, 18.1
L700	142	0.60	3.0, 17.7
C450	288	0.76	7.8
C600	247	0.74	8.5
C700	144	0.88	12.3

[a] The specific surface areas (S_{BET}) were calculated using nitrogen adsorption data in the range of relative pressure 0.05−0.30 according to a BET method, and total pore volume (V_p) was estimated from the adsorption data at $p/p_0 = 0.99$. Pore size was estimated by applying a BJH method to the desorption isotherm of the corresponding calcined samples.

isotherms of samples C450 and C600 (Figure 8b) are of type IV with type H2 hysteresis loops, suggesting characteristics of mesoporous materials according to IUPAC classification.[26] From BJH pore size distributions (Figure 9b), it can be observed that both samples exhibit a narrow size distribution in the range below 20 nm. This could be associated with the templating effect as a consequence of the removal of carbon from the hybrid precursor. Large amounts of in situ "co-generated" carbon particles as templates, uniformly and highly dispersed into LDHs matrixes in the composite precursor, effectively separate the LDH crystallites. As a result, the porous mixed oxides are obtained after the removal of carbon template with the elevated temperatures, resulting in narrow pore size distributions and high surface areas. The monomodal pore characteristic in the pore size distribution further reveals the role of carbon as template, in that the crystallization of LDH and the simultaneous in situ generation of carbon lead to a highly hybridized composite precursor. Such a structure is favorable to the formation of mesopore network with small pores and a narrow pore size distribution after removal of the carbon. The specific surface areas of samples C450 and C600 (Table 1) are as high as 288 and 247 m^2 g^{-1}, respectively, much higher than those of L450 and L600. This can be attributable to the mesopore network and the small pore sizes of samples, which is consistent with the above TEM observations (Figure 7d and e). In addition, the pore size maximum of C600 has a slight increase than that of C450, thus leading to a decrease in

(26) Leofanti, G.; Padovan, M.; Tozzola, G.; Venturelli, B. *Catal. Today* **1998**, *41*, 207.

Table 2. Textural Properties of the Mixed-Metal Oxides after a Reduction Treatment[a]

sample	S_{BET} (m^2 g^{-1})	V_p (cm^3 g^{-1})	pore size (nm)
L450RE	92	0.56	18.1
L600RE	80	0.52	17.2
C450RE	190	1.35	12.4
C600RE	155	1.23	12.5

[a] The specific surface areas (S_{BET}) were calculated using nitrogen adsorption data according to a BET method, and total pore volume (V_p) was estimated from the adsorption data at $p/p_0 = 0.99$. Pore size was estimated by applying the BJH method to the desorption branch of the isotherms.

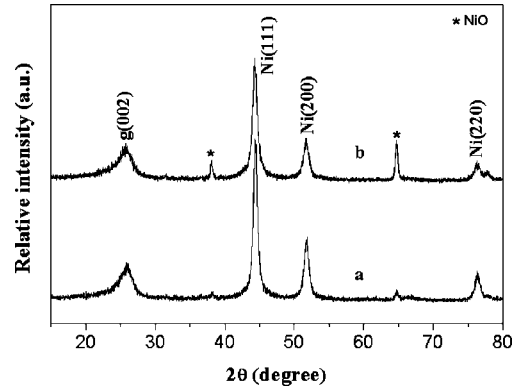

Figure 10. XRD patterns of purified CNTs over (a) sample C450 and (b) sample C600.

specific surface areas. However, the textural properties of sample C700 calcined at higher temperature show different features, compared with those of C450 and C600. The surface area decreases remarkably and the pore sizes increase (Table 1). It can be ascribed to the aggregates of larger NiO particles and the breakage of mesopore network to some extent. This is agreement with the TEM photograph (Figure 7f). Therefore, the control of texture can be expected via a temperature-mediated templating approach. It is worth noting that the total pore volume of sample C700 is larger than those of other two samples calcined at lower temperatures, mostly because of the existence of the larger voids among large particles.

The difference in textural properties of the mixed oxides derived from different precursors probably originates from the formation mechanism of porous structure. Commonly, the layered LDHs or intercalated LDHs transform into mixed oxides with three-dimensional texture and porous channels by the elimination of interlamellar anions and the collapse of layers after calcination. The textural properties of the resulting mixed oxides can vary with the types of cations and anions as well the contents, which is a prevailing way to adjust the surface areas and porosity.[27] In our case, the mixed oxides derived from a kind of LDH/C composite precursor have distinctly different structural and textural properties, compared to those derived from pristine LDH precursor. The conversion from the composite precursor to porous mixed oxides is described as follows. First, carbon as a "co-generated template" in the composite confines the small crystalline size of LDH and prevents the agglomeration of LDH particles by assembling LDH sheets with the formed

(27) Xu, Z. P.; Zeng, H. C. *Chem. Mater.* **2000**, *12*, 3459.

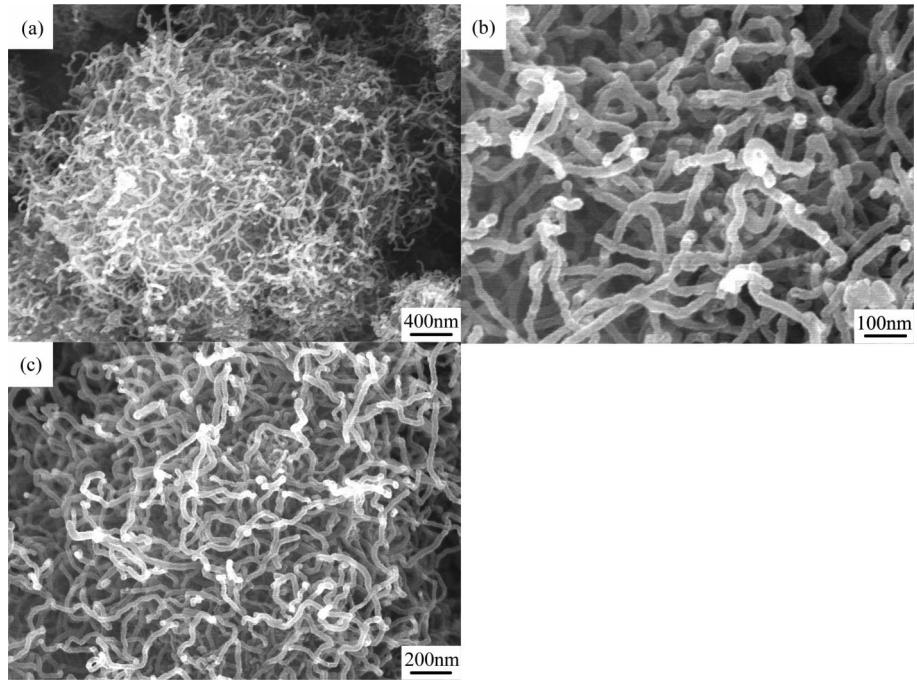

Figure 11. SEM images of CNTs grown over (a) sample C450, (b) a magnified view, and (c) over sample C600.

carbon, i.e., the composite effect of hybrid structure. Second, the layered LDH is gradually transformed into mixed oxides with elevated temperatures, simultaneously accompanied by elimination of carbon due to oxidation in air ambient. Herein, the carbon as "sacrificial template" further plays a critical role in the formation of mesoporous mixed oxides with high surface area and narrow pore size distribution via an evacuation process in mesoscale. A kind of mesoporous network can be created and maintained at an appropriate calcination temperature in view of the close connections among the resulting particles. Finally, upon further elevating the temperature, the mesopore network is destroyed and well-crystalline NiO phase is born in the products through recrystallization.

On the other hand, according to TEM photograph of L450RE (see the Supporting Information, Figure S1a), only some aggregates composed of particles of 10–20 nm are observed, suggesting that the reduction destroys the platelike morphology of calcined pure LDH. In contrast, sample C450RE still retains the mesopore network characteristic to some extent (see the Supporting Information, Figure S1b), although the network continuity is partially broken down because of the existence of some larger voids in the structure resulting from the formation of metallic Ni particles in the mixed oxides. Furthermore, the isotherms of C450RE and C600RE samples (see the Supporting Information, Figure S2) exhibit type III characteristics with a type H3 loop, indicative of essentially mesoporous character with the pore size distribution extending into the macropore regime.[9b,28] This result is consistent with the TEM observation. Importantly, C450RE and C600RE samples have surface areas of 190 and 155 $m^2\ g^{-1}$ (Table 2), much higher than their corresponding carbon-free counterparts.

Catalytic Property for CNT Growth. It is well-known that the formation of CNTs by catalytic chemical vapor deposition (CCVD) occurs through the catalytic decomposition of a carbonaceous gas over nanometric metal particles. Typically, they are transition metals (iron, nickel, cobalt) dispersed and stabilized over large-surface-area solid supports such as metal oxides, silica, or various types of zeolites.[29] Therefore, it is expected that the mesoporous nickel-based mixed oxides could exhibit good catalytic activities for the growth of CNTs because of their high surface areas and the distribution of a catalytically active component.

The XRD patterns of purified products over the samples C450 and C600 were shown in Figure 10. The diffraction peak appearing at 25.8° can be assigned to graphitic carbon (002) diffraction as g(002), indicative of the existence of carbon product. In addition, several intensive peaks at 44.3, 51.8, and 76.2° correspond to the metallic Ni (111), (200), and (220) diffractions, respectively (JCPDS 87–0712). The remaining NiO phase (JCPDS 47–1049) is still detected. According to Scherrer's formula, the crystallite size of metallic Ni is estimated to be around 12 nm for C450 and 10 nm for C600, which may foster effective catalytic capability for CNT growth. Figure 11 exhibits the overall morphology of as-grown CNTs over the catalysts. It can be seen that a large quantity of tubular structures were densely grown over the sample C450 (Figure 11a). The magnified view, in Figure 11b, displays a clearer morphology of nanotubes with uniform diameter. A similar feature was observed for CNTs over the sample

(28) Gregg, S. J. *Colloids Surf.* **1986**, *21*, 109.

(29) (a) Pinheiro, J. P.; Schouler, M. C.; Gadelle, P.; Mermoux, M.; Dooryhee, E. *Carbon* **2000**, *38*, 1469. (b) Li, Y.-L.; Kinloch, I. A.; Shaffer, M. S. P.; Singh, C.; Geng, J.; Johnson, B. F. G.; Windle, A. H. *Chem. Mater.* **2004**, *16*, 5637. (c) Takenaka, S.; Ishida, M.; Serizawa, M.; Tanabe, E.; Otsuka, K. *J. Phys. Chem. B* **2004**, *108*, 11464. (d) Takenaka, S.; Orita, Y.; Matsune, H.; Tanabe, E.; Kishida, M. *J. Phys. Chem. C* **2007**, *111*, 7748.

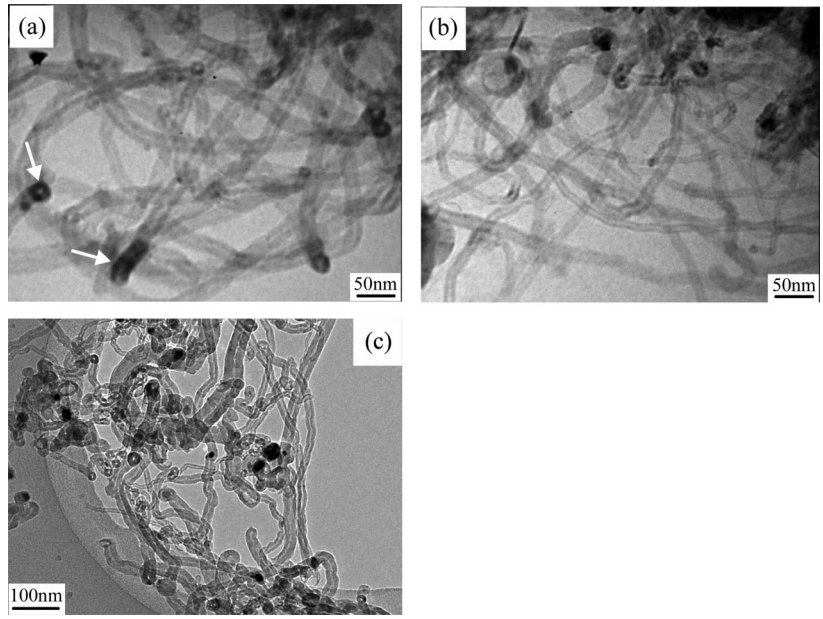

Figure 12. TEM photographs of as-grown CNTs over sample (a) C450, (b) sample C600, and (c) sample L600.

C600 (Figure 11c). Figure 12a shows a TEM photograph of CNTs grown over the sample C450. Similarly, these nanotubes exhibit a uniform outer diameter of ca. 20 nm, in good agreement with the SEM observations, and display a continuously hollow structure inside the nanotube. A common feature, apparently, was found in which spherical particles are attached to the ends of nanotubes (highlighted by white arrows), suggestive of their catalytic growth mode. The CNTs grown over the sample C600 show smaller diameters (ca. 17 nm) than those over the sample C450 (Figure 12b), which is consistent with the crystallite size of Ni particles estimated by XRD data.

On the other hand, the diffraction at 25.9° in the XRD pattern of purified CNTs over L600 sample (see the Supporting Information, Figure S3) also confirms the formation of graphitic carbon. The crystallite size of Ni is calculated to be 17 nm using Scherrer's formula, larger than the value from the XRD pattern of CNTs over the C600 (10 nm), which can be ascribed to lower dispersion of reduced Ni clusters resulting from the lower surface area of L600. It is noted from Figure 12c that the CNTs grown over L600 have larger diameters and a wider distribution than those over C600. In addition, a number of nontubular structures composed of particle-encapsulated carbon were found. The result indicates that sample L600 is unfavorable to the growth of tubular graphite structures because of the formation of larger metal particles after reduction.

Figure 13 shows Raman spectra of the CNTs over L600 and C600. Two strong bands at 1350 and 1589 cm^{-1} correspond to the D and G bands of the typical Raman peaks of graphitized carbon nanotubes, respectively. The D band is attributed to the structural disorder or the presence of amorphous carbon. The G band is related to the vibration of sp^2-bonded carbon atoms in a two-dimensional hexagonal lattice, indicative of formation of ordered graphite layers. It is known that the smaller ratio of

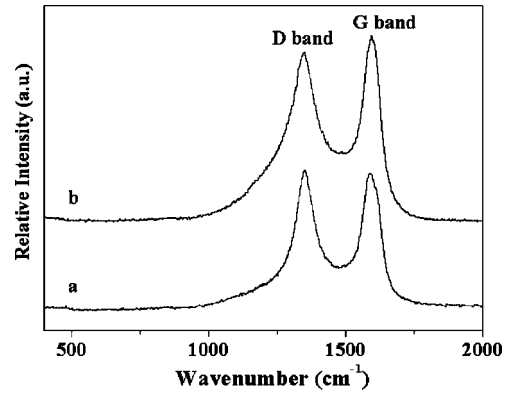

Figure 13. Raman spectra of the CNTs over (a) sample L600 and (b) sample C600.

I_D/I_G reflects the higher ordering of the graphite phase.[30] Obviously, the CNTs grown over C600 with the I_D/I_G ratio of 0.90 have a higher degree of graphitization than those over L600 with the I_D/I_G ratio of 1.03. This is due to the fact that the mesopore networks as well as the high surface area of C600 lead to the formation of highly dispersed metallic Ni nanoparticles after reduction, thus giving rise to uniform diameters of CNTs and less amorphous carbon.

Conclusions

Ni−Al layered double hydroxide/carbon composite with a hybrid structure has been successfully assembled under mild and environmentally benign hydrothermal conditions. The thermal conversion of composite precursor produces high surface areas Ni-based mixed oxides with interconnected mesopore networks at calcination temperature of 450 °C or above. The templating effect of in situ generated carbon by the carbonization of glucose in the hybrid materials plays a key

(30) Reich, S.; Thomsen, C.; Maultzsch, J. *Carbon Nanotubes: Basic Concepts and Physical Properties*; Wiley-VCH: Weinheim, Germany, 2004.

role for the formation of mesoporous solids with narrow size distributions. The well-defined NiO nanoparticles could form in the mixed oxides upon heat treatment at higher temperature. The catalytic results show that as-prepared mesoporous Ni-based mixed oxides exhibit excellent catalytic activities for CNT growth. Such a tunable mesopore network of Ni-based mixed oxides should be desirable in a more extensive field of heterogeneous catalysis. In addition, the synthesis strategy described here might provide a new and facile route to fabricate various specific metal oxide materials concerned with interconnected mesopore systems at low cost and without use of specialized mesoporous templates, based on the widely used layered double hydroxides materials. And the unique structural and textural properties of resulting materials can lead to the enhanced performance in catalysis, decontamination, and sensing.

Acknowledgment. The authors gratefully acknowledge the financial support from the National Natural Science Foundation of China (20601002, 20631040), the Program for Changjiang Scholars and Innovative Research Team in University (IRT0406), 111 Project (B07004), the Program for New Century Excellent Talents in University (NCET-04-0120), and the Young Scholars Fund of Beijing University of Chemical Technology (QN0619).

Supporting Information Available: Additional TEM photographs of L450RE and C450RE samples, N_2 sorption isotherms and pore size distributions of C450RE and C600RE samples, and XRD pattern of the CNTs over L600 sample (PDF). This information is available free of charge via the Internet at http://pubs.acs.org.

CM702072T